

## *PSEN1ΔE9*, *APP<sup>swe</sup>*, and *APOE4* Confer Disparate Phenotypes in Human iPSC-Derived Microglia

Henna Konttinen,<sup>1</sup> Mauricio e Castro Cabral-da-Silva,<sup>2</sup> Sohvi Ohtonen,<sup>1</sup> Sara Wojciechowski,<sup>1</sup> Anastasia Shakirzyanova,<sup>1</sup> Simone Caligola,<sup>3</sup> Rosalba Giugno,<sup>3</sup> Yevheniia Ishchenko,<sup>1</sup> Damián Hernández,<sup>4,5,6</sup> Mohammad Feroze Fazaludeen,<sup>1</sup> Shaila Eamen,<sup>1</sup> Mireia Gómez Budia,<sup>1</sup> Ilkka Fagerlund,<sup>1</sup> Flavia Scoyni,<sup>1</sup> Paula Korhonen,<sup>1</sup> Nadine Huber,<sup>1</sup> Annakaisa Haapasalo,<sup>1</sup> Alex W. Hewitt,<sup>4,5,7</sup> James Vickers,<sup>8</sup> Grady C. Smith,<sup>2</sup> Minna Oksanen,<sup>1</sup> Caroline Graff,<sup>9,10</sup> Katja M. Kanninen,<sup>1</sup> Sarka Lehtonen,<sup>1</sup> Nicholas Propson,<sup>11</sup> Michael P. Schwartz,<sup>12</sup> Alice Pébay,<sup>4,5,6</sup> Jari Koistinaho,<sup>1,13</sup> Lezanne Ooi,<sup>2</sup> and Tarja Malm<sup>1,\*</sup>

<sup>1</sup>A.I.Virtanen Institute for Molecular Sciences, University of Eastern Finland, Kuopio 70211, Finland

<sup>2</sup>School of Chemistry and Molecular Bioscience, Illawarra Health and Medical Research Institute, University of Wollongong, Wollongong, NSW 2522, Australia

<sup>3</sup>Department of Computer Science, University of Verona, Verona 37134, Italy

<sup>4</sup>Centre for Eye Research Australia, Royal Victorian Eye and Ear Hospital, Melbourne, VIC 3002, Australia

<sup>5</sup>Department of Surgery, the University of Melbourne, Melbourne, VIC 3002, Australia

<sup>6</sup>Department of Anatomy and Neuroscience, the University of Melbourne, Melbourne, VIC 3002, Australia

<sup>7</sup>School of Medicine, Menzies Institute for Medical Research, University of Tasmania, Hobart, VIC 7005, Australia

<sup>8</sup>Menzies Institute for Medical Research, School of Medicine, University of Tasmania, Hobart, VIC 7005, Australia

<sup>9</sup>Department NVS, Division of Neurogeriatrics, Karolinka Institutet, Stockholm 17176, Sweden

<sup>10</sup>Theme Aging, Genetics Unit, Karolinka University Hospital-Solna, Stockholm 17176, Sweden

<sup>11</sup>Department of Molecular and Cell Biology and the Huffington Center on Aging, Baylor College of Medicine, Houston, TX 77030, USA

<sup>12</sup>Department of Chemistry, University of Wisconsin-Madison, Madison, WI 53706, USA

<sup>13</sup>Neuroscience Center, University of Helsinki, Helsinki 00014, Finland

\*Correspondence: [tarja.malm@uef.fi](mailto:tarja.malm@uef.fi)

<https://doi.org/10.1016/j.stemcr.2019.08.004>

### SUMMARY

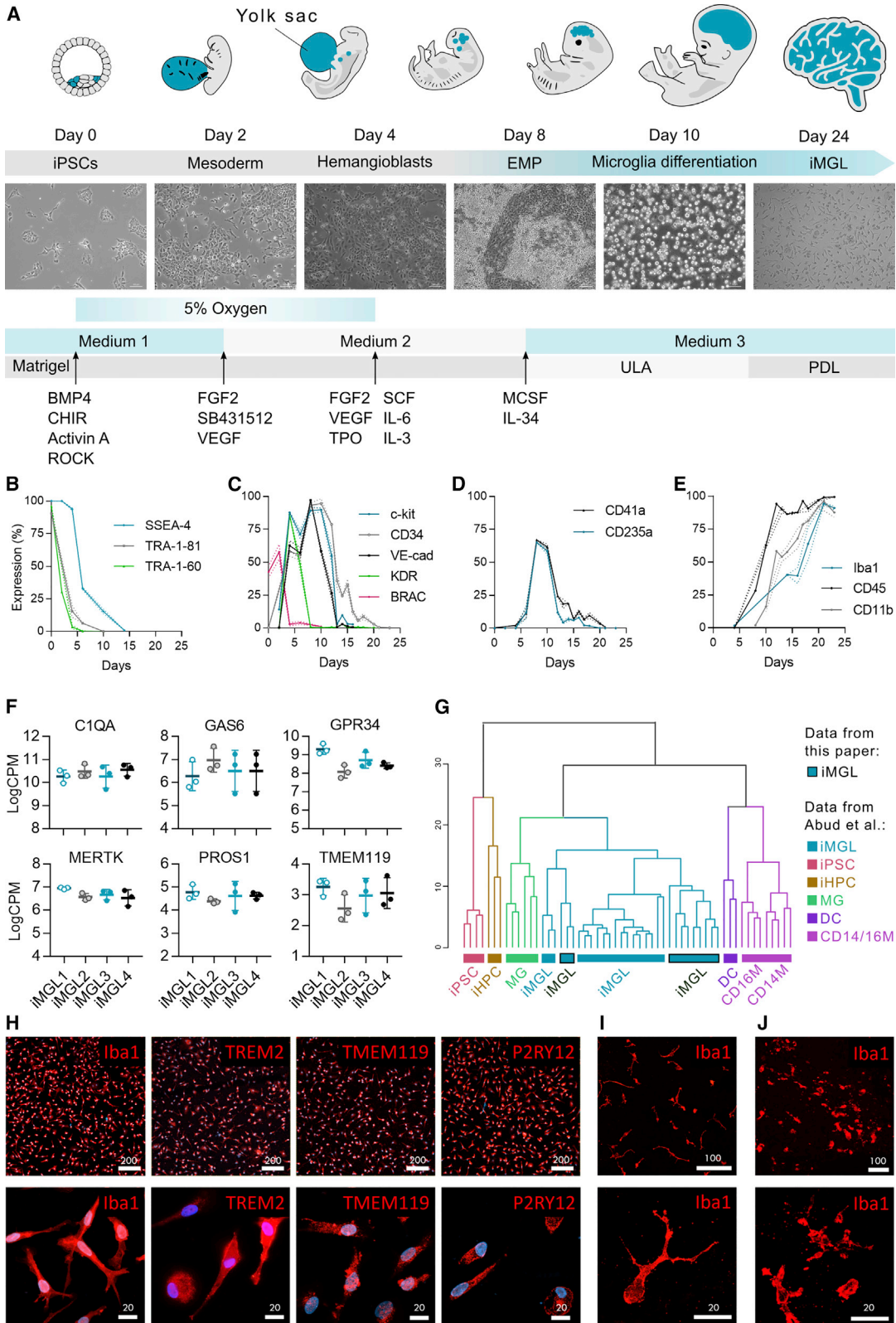
Here we elucidate the effect of Alzheimer disease (AD)-predisposing genetic backgrounds, *APOE4*, *PSEN1ΔE9*, and *APP<sup>swe</sup>*, on functionality of human microglia-like cells (iMGLs). We present a physiologically relevant high-yield protocol for producing iMGLs from induced pluripotent stem cells. Differentiation is directed with small molecules through primitive erythromyeloid progenitors to re-create microglial ontogeny from yolk sac. The iMGLs express microglial signature genes and respond to ADP with intracellular Ca<sup>2+</sup> release distinguishing them from macrophages. Using 16 iPSC lines from healthy donors, AD patients and isogenic controls, we reveal that the *APOE4* genotype has a profound impact on several aspects of microglial functionality, whereas *PSEN1ΔE9* and *APP<sup>swe</sup>* mutations trigger minor alterations. The *APOE4* genotype impairs phagocytosis, migration, and metabolic activity of iMGLs but exacerbates their cytokine secretion. This indicates that *APOE4* iMGLs are fundamentally unable to mount normal microglial functionality in AD.

### INTRODUCTION

Alzheimer disease (AD) is a progressive neurodegenerative disorder and the most common cause of dementia (Weuve et al., 2014). AD pathology begins decades before the onset of clinical symptoms and neuroinflammation is strongly indicated in its progression (Shi and Holtzman, 2018). Neuroinflammation is mediated by microglia, the innate immune cells of the CNS. Microglia originate from erythromyeloid progenitor cells (EMPs) in the embryonic yolk sac (Ginhoux et al., 2013) and play pivotal roles in CNS development, as well as in tissue maintenance, injury response, and pathogen defense (Colonna and Butovsky, 2017). In AD, microglia are aberrantly activated and their normal functions are compromised (Saijo and Glass, 2011).

The major genetic risk factor for multifactorial late-onset AD (LOAD) (Liu et al., 2013) is a gene variant apolipoprotein E4 (*APOE4*), whereas inherited genetic mutations in

presenilin 1 (*PSEN1*), presenilin 2 (*PSEN2*), or amyloid precursor protein (*APP*) genes (Selkoe, 1998) cause rarer early-onset familial AD (FAD) (Bagyinszky et al., 2014). Human *APOE* is primarily expressed in three variants, the most abundant *APOE3* being neutral, and the rarest *APOE2* being protective in AD. All forms are involved in transport and elimination of lipids, but a common mode of action in the brain remains largely unexplored. *APOE* is highly expressed in microglia, and *APOE4* is shown to promote the neurodegeneration-associated inflammatory phenotype of mouse microglia (Krasemann et al., 2017) and alter functions of human microglia-like cells (iMGLs) (Lin et al., 2018). However, the precise role of *APOE4* in the development of AD remains elusive. *PSEN1* and *APP* participate in the production of neurotoxic amyloid-beta (Aβ) peptide, the main component of the amyloid plaques found in the brains of AD patients. The expression of *APP* and *PSEN1* in microglia is shown to increase upon brain insults (Banati



(legend on next page)



et al., 1993; Nadler et al., 2008) and these genes are implicated in inflammatory processes (Manocha et al., 2016; Zhao et al., 2017), but it is unclear whether they contribute to AD through microglial functions.

Given the central role of microglia in AD and the lack of knowledge of FAD mutations or *APOE4* in human microglia, we established a method to generate iMGLs from induced pluripotent stem cells (iPSCs) carrying *APOE4* genotype or *PSEN1ΔE9* or *APPswe* mutations. iMGLs have a robust microglial phenotype and resemble recently published iPSC-derived microglia (Abud et al., 2017; Douvaras et al., 2017; McQuade et al., 2018). We conclude that *APOE4* genotype has a substantial impact on the function of iMGLs, whereas the FAD mutations have only minor effects. *APOE4* contributes particularly to reduced migration, increased proinflammatory responses and defective glycolytic and mitochondrial metabolism. This study elucidates the role of human microglia in disease pathogenesis in FAD and LOAD.

## RESULTS

### iPSCs Differentiate into iMGLs through Primitive Hematopoiesis

We developed a high-yield 24-day protocol to differentiate human iPSCs into iMGLs. To recapitulate microglial ontogeny from the yolk sac (Ginhoux et al., 2010; Kierdorf et al., 2013; Schwartz et al., 2015; Uenishi et al., 2014), we used small molecules under defined oxygen conditions to direct differentiation through primitive EMPs followed by microglial maturation (Figure 1A). Morphological changes and the expression of the key markers for each stage of differentiation were assessed by flow cytometry and phase-contrast microscopy (Figures 1B–1E and S1).

During the first differentiation days (D0–2), mesodermal lineage was induced with BMP4, Activin A and CHIR99021 under low oxygen (5% O<sub>2</sub>) conditions and was accompanied with a reduction of pluripotency markers (Figure 1B). When the expression of mesodermal brachyury was the highest, 48 h after initiation (Figure 1C), basic fibroblast growth factor (bFGF), SB431542, vascular endothelial growth factor (VEGF), and insulin were applied to evoke

hemogenic differentiation. Subsequently, the areas of endothelial-like cells formed (Figure S1) and the expression of hemogenic EMP markers KDR, CD117 (c-kit), VE-cadherin, and CD34 increased (Figure 1C). On D6–7, loosely attached round cells appeared with a high expression of primitive EMP markers CD235a (Sturgeon et al., 2014) and CD41a (Kennedy et al., 2007) (Figure 1D). MCSF1 and interleukin-34 (IL-34) were used to induce microglial differentiation and expansion on ultra-low attachment (ULA) dishes. On maturation, the expression of myeloid markers increased and on D24, 88% of cells expressed CD11b, 99% CD45, and 91% IBA1 when cultured on ULA dishes (Figure 1E). To mature iMGLs for functional experiments, D16 progenitors were cultured on poly-D-lysine (PDL)-coated vessels until D24 to promote ramified and elongated morphology and IBA1 expression (Figure S1).

The microglial identity of iMGLs was confirmed with whole-transcriptome analysis and qRT-PCR (Figures 1F and S2; Table S1). The microglial signature genes, *C1QA*, *GAS6*, *GPR34*, *MERTK*, *PROS1*, and *TMEM119* (Butovsky et al., 2014), were highly expressed (logCPM>2, Figures 1F and S2). Comparison of RNA sequencing profiles to published dataset GSE89189 (Abud et al., 2017) using microglia genes (Lavin et al., 2014) revealed that iMGLs cluster with published iPSC-derived microglia (Abud et al., 2017), as well as with human microglia (Zhang et al., 2014), but remain distinct from iPSCs and other tissue myeloid cells (Figures 1G and S2). Immunostaining of D24 iMGLs verified ubiquitous expression of IBA1, CX3CR1, and PU.1 (Figures 1H and S1) and, importantly, microglia-specific proteins TMEM119, P2RY12, and TREM2 (Bennett et al., 2016) (Figure 1H). Furthermore, iMGLs spontaneously migrated into 3D co-cultures and adopted a ramified morphology (Figures 1I and 1J). Thus, the iMGLs generated through induction of primitive EMPs show a typical microglia-like genetic signature and protein expression.

### iMGLs Express *APP* and *PSEN1*, and *PSEN1ΔE9* Mutation Leads to Expected Alterations in *PSEN1* Endoproteolysis

To assess the reproducibility of the differentiation protocol, we successfully generated iMGLs from 16 different iPSC

### Figure 1. iPSCs Differentiate into iMGLs through Primitive Hematopoiesis

(A–E) Schematic protocol (A). Percentages of positive cells analyzed by flow cytometry for markers of (B) pluripotency, (C) EMPs and mesodermal brachyury (BRAC), (D) primitive EMPs, and (E) and mature microglia. n = 4 cell lines, repeated in 3 batches. (F) The expression of microglial signature genes in RNA sequencing (RNA-seq) data of D24 iMGLs as log<sub>2</sub> CPM values. n = 3 batches, 4 cell lines. (G) Hierarchical clustering of RNA-seq data shows that our iMGLs cluster with published iMGLs and human microglia (MG), but are distinct from dendritic cells (DCs), monocytes (CD14M and CD16M), iPSCs, and hematopoietic progenitor cells (HPCs) (Abud et al., 2017). (H–J) Immunostainings of D24 iMGLs (H). Repeated with two batches for all cell lines. Images of iMGLs labeled with IBA1 (red) in (I) 3D-Matrigel co-culture with neurons and in (J) cerebral brain organoids. Repeated with two batches for 2–4 cell lines. Scale bars as μm. Data presented mean ± SEM.

See also Figures S1 and S2; Tables S1 and S2.

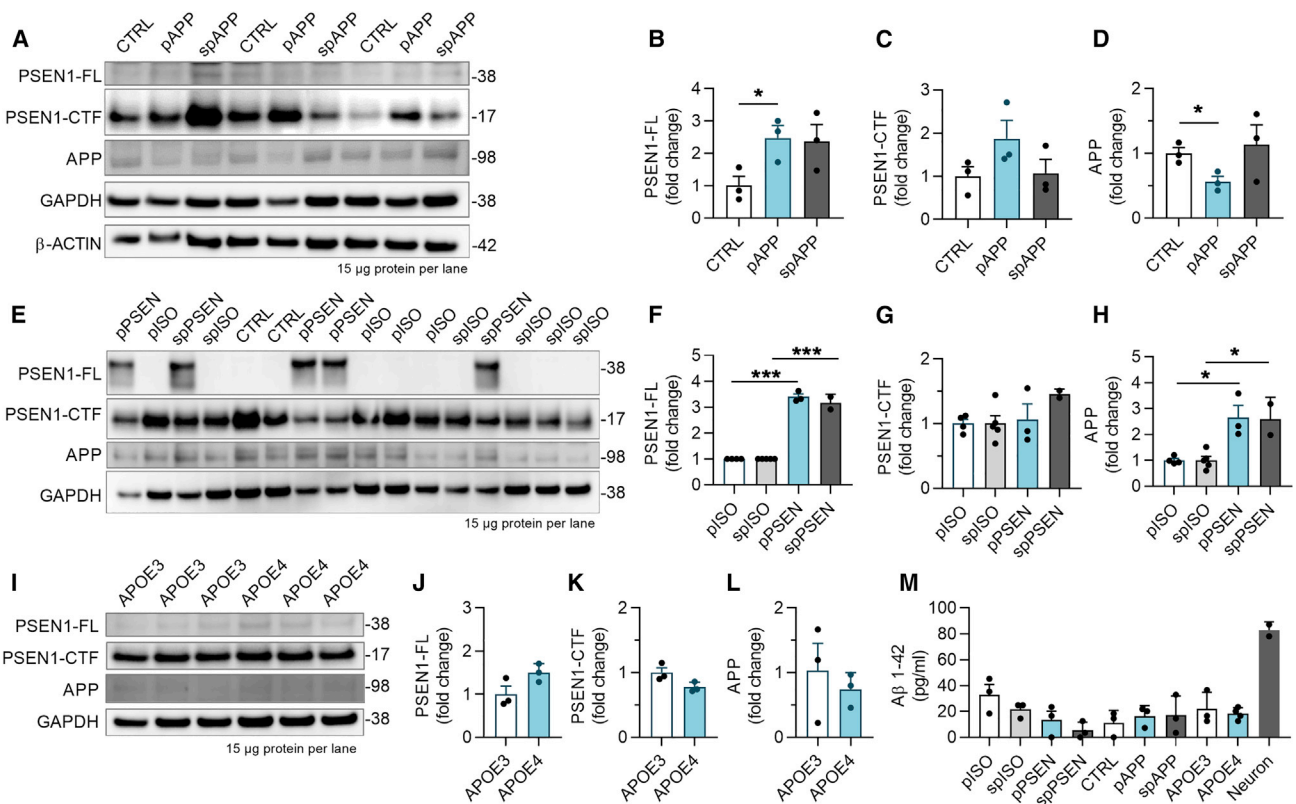


**Figure 2. iMGLs Express APP and PSEN1 Proteins, and *PSEN1* $\Delta$ E9 Mutation Leads to Expected Alterations in PSEN1 Endoproteolysis** (A–L) Western blots for full-length (FL) and C-terminal fragment (CTF) of PSEN1 and APP proteins from 3 batches of control (CTRL) and *APP**swe* (pAPP, spAPP) iMGLs (A). GAPDH and b-ACTIN as loading controls. Quantification of blots normalized to GAPDH for (B) PSEN1-FL, (C) PSEN1-CTF, and (D) APP protein. *n* = 3 batches. Respective western blots (E) and quantification (F–H) for *PSEN1* $\Delta$ E9 iMGLs (pPSEN, spPSEN) and their isogenic controls (pISO and spISO). *n* = 2–5 batches. Western blots (I) for *APOE3* and *APOE4* iMGLs and quantification (J–L) for the proteins. *n* = 3 batches.

(M) A $\beta$  1–42 levels in cell culture medium after 48 h analyzed by ELISA. *n* = 2–5 batches for *APP* and *PSEN1*; *n* = 3 wells for *APOE* repeated in three batches.

Data presented mean  $\pm$  SEM unpaired two-tailed t test, \**p* < 0.05, \*\**p* < 0.01, \*\*\**p* < 0.001. p, presymptomatic; sp, symptomatic. See also Figure S3.

lines (Table S3) with a 20-fold average yield. iPSCs originated from adult donors. Neutral *APOE* $\epsilon$ 3/3 alleles (*APOE3*) were carried by five healthy subjects, two subjects with familial KM670/671NL Swedish double mutation in *APP* (*APP**swe*) (Mullan et al., 1992), and two with a familial 4.6-kb deletion of exon 9 in *PSEN1* (*PSEN1* $\Delta$ E9) (Crook et al., 1998). Three subjects carried *APOE* $\epsilon$ 4/4 alleles (*APOE4*) (Balez et al., 2016; Engel et al., 2018; Munoz et al., 2018; Ooi et al., 2013). One *APP**swe* carrier had symptomatic AD (referred spAPP) and one was presymptomatic (pAPP) with no clinical diagnosis. Similarly, one *PSEN1* $\Delta$ E9 carrier was presymptomatic (pPSEN) and one had AD diagnosis (spPSEN). The effect of *PSEN1* $\Delta$ E9 mutation was validated with gene-corrected isogenic control lines from the symptomatic (spISO) and the presymptomatic (pISO) *PSEN1* $\Delta$ E9 carriers (Oksanen et al., 2017). Pluripo-

tency and the karyotype of previously unpublished pAPP, *APOE3*, and *APOE4* lines were characterized (Figure S3).

We next analyzed the effect of genetic background on processing of APP protein into toxic A $\beta$ . *APP**swe* iMGLs showed 2.5-fold increase in PSEN1 protein but no consistent changes in APP compared with control cells (Figures 2A–2D). As expected, *PSEN1* $\Delta$ E9 iMGLs showed a robust accumulation of PSEN1 and a 3-fold increase in APP compared with isogenic controls (Figures 2E–2H), thereby establishing that the *PSEN1* $\Delta$ E9 mutation resulted in a loss of  $\gamma$ -secretase cleavage of APP. Furthermore, *APOE3* and *APOE4* lines showed low levels of APP, PSEN1, and C-terminal fragments of PSEN1, and no differences between the genotypes (Figures 2I–2L). Quantification of A $\beta$  fragments from cell lysates and culture media revealed that iMGLs had no intracellular A $\beta$  and secreted only

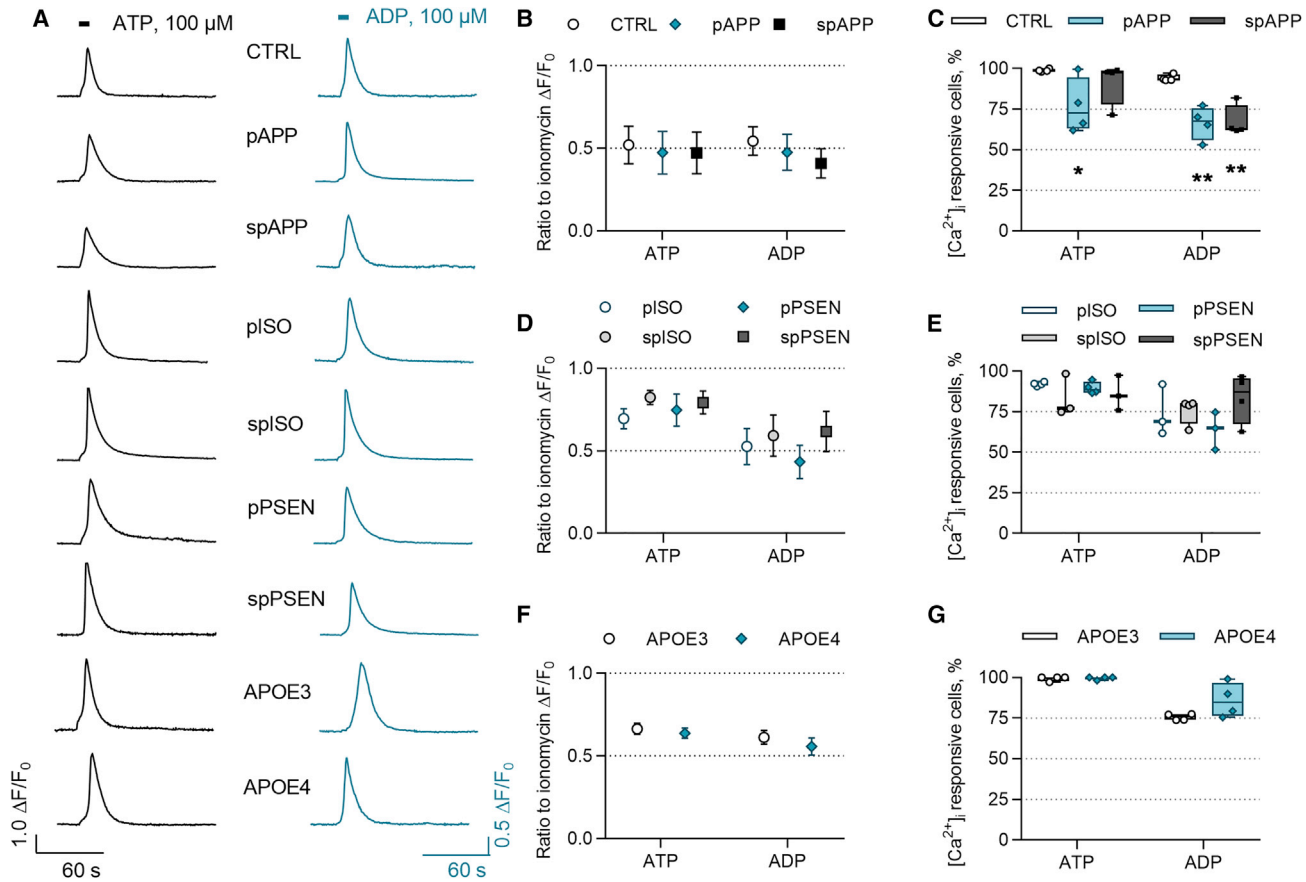


### Figure 3. ATP and ADP Evoke Intracellular Calcium [Ca<sup>2+</sup>]<sub>i</sub> Transients in iMGLs

(A) Example traces of [Ca<sup>2+</sup>]<sub>i</sub> transients following 100 μM ATP (left panel) and ADP (right panel) applications for 5 s (indicated by bars) in iMGLs loaded with the Ca<sup>2+</sup> indicator Fluo-4 AM.

(B) The ratio of maximum amplitudes normalized to amplitudes evoked by ionomycin that was applied in the end of experiment and used as inclusion criteria. n = 4 batches, each with 9–10 coverslips, altogether 3,994 CTRL, 3,015 pAPP, and 3,906 spAPP cells.

(C–E) Percentages of ATP- and ADP-responsive cells in *APPswe* lines compared with control iMGLs (C). Ratio of maximum amplitudes (D) and percentages of responsive cells (E) obtained from isogenic and *PSEN1ΔE9* iMGLs. n = 4 batches, each with 9–12 coverslips, altogether 1,969 pISO, 2,355 spISO, 1,856 pPSEN, and 2,823 spPSEN cells.

(F and G) Similar data for *APOE3* and *APOE4* iMGLs. n = 4 coverslips, altogether 482 *APOE3* and 991 *APOE4* cells, repeated in three batches. Data presented mean ± SEM unpaired two-tailed t test or one-way ANOVA followed by Bonferroni's post hoc test, \*p < 0.05, \*\*p < 0.01. CTRL, control; p, presymptomatic; sp, symptomatic; PSEN, *PSEN1ΔE9*; APP, *APPswe*; and ISO, isogenic control iMGLs.

Aβ<sub>1-42</sub> at similar levels regardless of the genotype (Figure 2M). Taken together, all cell lines had a normal karyotype and expressed FAD mutations or LOAD risk variants supporting their use for studying AD, even though genotypes failed to alter iMGL Aβ production.

### ATP and ADP Evoke Intracellular Calcium Transients in iMGLs

Since calcium may control microglial functions under resting and activated conditions (Hoffmann et al., 2003), we next investigated intracellular calcium [Ca<sup>2+</sup>]<sub>i</sub> transients in response to ATP and ADP. The representative traces of [Ca<sup>2+</sup>]<sub>i</sub> transients demonstrate similar responses in all

genotypes (Figure 3A). The average amplitudes of the responding cells were equal in control and *APPswe* iMGLs (Figure 3B). In contrast, there was a 22% reduction in ATP-responsive cells in pAPP iMGLs and a 27% reduction in ADP-responsive cells in both pre- and symptomatic *APPswe* iMGLs compared with control (Figure 3C). Equal amplitudes and percentages of responsive cells were observed for isogenic and *PSEN1ΔE9* iMGLs (Figures 3D and 3E), and for *APOE3* and *APOE4* iMGLs (Figures 3F and 3G) demonstrating the consistent functionality of iMGLs harboring these genotypes. Collectively, all cell lines responded to ADP and ATP by intracellular calcium release, supporting microglia-like functionality of the

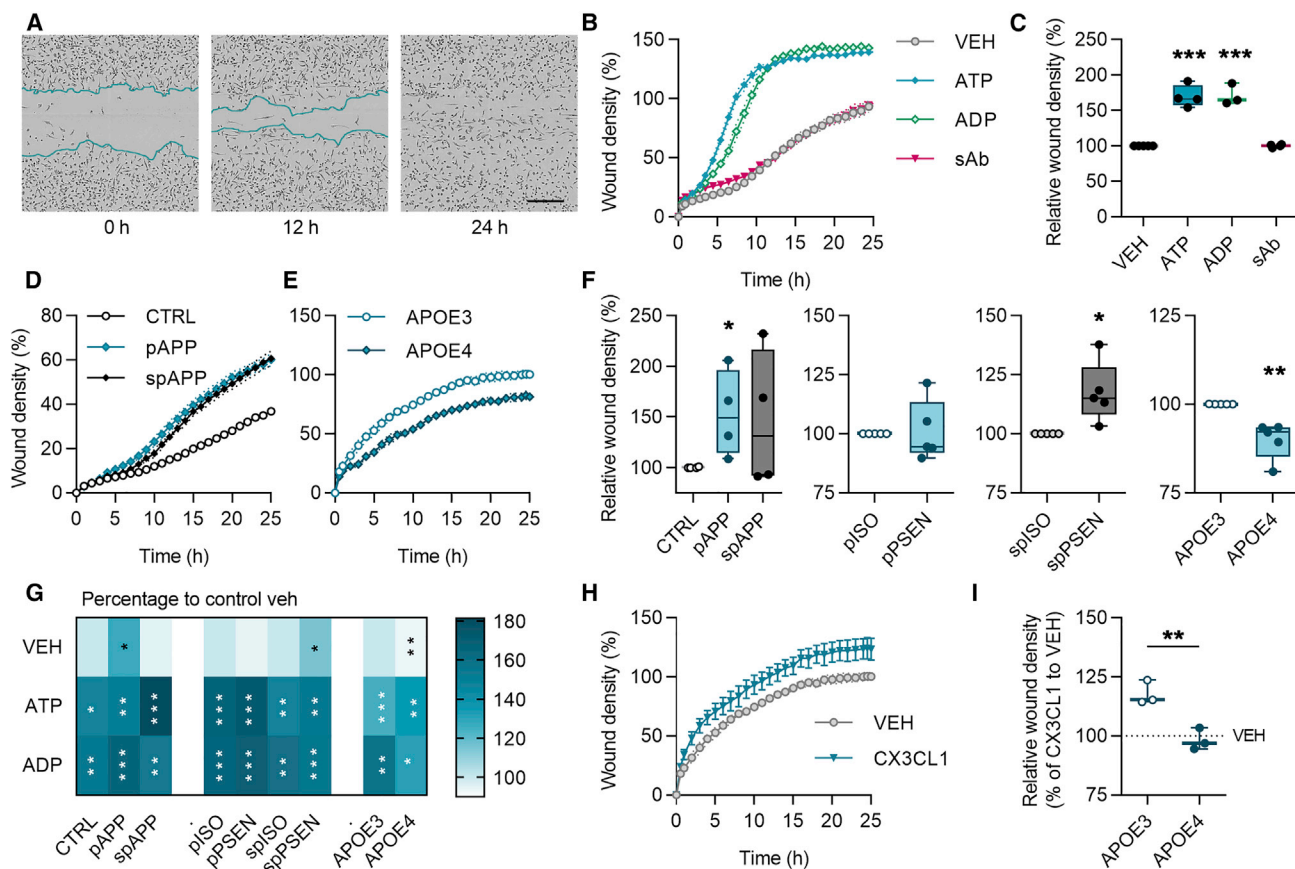


**Figure 4. Chemokinesis Is Accelerated in *APPswe* and *PSEN1ΔE9* iMGLs but Decelerated in *APOE4* iMGLs**

(A) Representative images of iMGLs in scratch wound migration assay at 0, 12, and 24 h time points. Scale bar 300  $\mu$ m. (B) Wound densities measured for 25 h with vehicle (VEH), 100  $\mu$ M ATP, 100  $\mu$ M ADP, or 1- $\mu$ M soluble sA $\beta$  treatments. (C–E) Wound densities at 24 h normalized to vehicle (C). Time curves for (D) control (CTRL) and *APPswe* (APP), and (E) *APOE3* and *APOE4* iMGLs. (F) Wound densities at 24 h normalized to control or isogenic (ISO) iMGLs. (G) A heatmap for increase (darker color) or decrease (lighter color) in wound density compared with vehicle. White asterisks indicate significance compared with vehicle and black asterisks to control genotype. (H) Time curves for wound density with 100  $\mu$ M fractalkine (CX3CL1) treatment in *APO3* iMGLs. (I) Corresponding wound density at 24 h normalized to vehicle for *APOE* iMGLs. Curve graphs show a representative experiment of three replicates, n = 3–5 wells. Boxplots and heatmap show normalized results from n = 3–5 replicate batches. Data presented mean  $\pm$  SEM, unpaired two-tailed t test, \*p < 0.05, \*\*p < 0.01, \*\*\*p < 0.001. p, presymptomatic; sp, symptomatic. See also Figure S4.

iMGLs. Reduction in *APPswe* responses suggests that FAD mutation can alter intracellular calcium signaling.

#### Chemokinesis Is Accelerated in *APPswe* and *PSEN1ΔE9* iMGLs but Decelerated in *APOE4* iMGLs

Microglial migration to the injury site is crucial for maintaining homeostasis in the brain. We analyzed the chemokinesis of iMGLs using a scratch wound assay with live-cell imaging for 24 h (Figure 4A). Acute application of ATP and ADP, which can be released from injured neurons, increased migration in all tested cell lines, whereas soluble oligomeric A $\beta$  (sA $\beta$ ) failed to alter migration (Figures 4B,

4C, and S4). We observed increased basal migration in *APPswe* lines compared with control iMGLs as well as in spPSEN iMGLs compared with their isogenic controls (Figures 4D, 4F, and S4). In contrast, *APOE4* genotype reduced basal migration (Figures 4E and 4F). ATP or ADP induced similar increase in migration in all genotypes (Figure 4G). In contrast, migration evoked by fractalkine was restrained in *APOE4* iMGLs compared with *APOE3* (Figures 4H and 4I), indicating impairment in motility in response to this neuron-derived chemokine. The migration was reduced if fetal bovine serum (FBS) was withdrawn from cell culture and therefore the experiments were performed in the



presence of FBS (Figure 4S). Overall, all iMGL lines migrated and responded to different stimuli as expected for microglia. A reduction in *APOE4* and a mild increase in APP and PSEN1 iMGLs suggest that LOAD risk variant and FAD mutations have different effects on microglial functions.

### Phagocytosis Is Dampened in *APOE4* iMGLs, but Not in *APP<sup>swe</sup>* or *PSEN1ΔE9* iMGLs

Since microglia fail to efficiently clear A $\beta$  plaques in AD (Lee and Landreth, 2010), we examined phagocytosis by live-cell imaging. iMGLs spontaneously phagocytosed pHrodo Zymosan A bioparticles (Figures 5A and 5B) equivalently despite of their genotypes (Figures 5C, 5D, and 54). Since *APOE4* variant was recently reported to reduce phagocytosis in iPSC-derived microglia (Lin et al., 2018), we investigated *APOE* iMGLs also with confocal microscopy and with fewer number of larger fluorescein isothiocyanate (FITC) Zymosan A bioparticles to count internalized particles (Figures 5E and 5F). Indeed, despite the equal overall intensity of phagocytosed pHrodo particles (Figure 5G), *APOE4* iMGLs ingested a smaller number of FITC particles per cell compared with *APOE3* (Figure 5H).

Next, we tested whether proinflammatory stimuli attenuate the phagocytosis of iMGLs as reported for murine microglia (Koenigsnecht-Talboo and Landreth, 2005). iMGLs were pretreated with lipopolysaccharide (LPS), interferon  $\gamma$  (IFN- $\gamma$ ), or both LPS and IFN- $\gamma$  (LPS-IFN- $\gamma$ ) for 24 h or treated with sA $\beta$  or insoluble fibrillary (fA $\beta$ ) A $\beta$ 1-42 at the time of particle application. Unexpectedly, LPS failed to alter phagocytosis of pHrodo beads, whereas IFN- $\gamma$  or LPS-IFN- $\gamma$  suppressed it (Figures 5I–5L). Withdrawal of stimuli before to the measurement did not restore IFN- $\gamma$ -mediated suppression, but in the LPS-pretreated group phagocytosis was first abrogated and then potentiated 5 h after withdrawal (Figure 54). Addition of fA $\beta$  only slightly enhanced the phagocytosis of pHrodo beads in presymptomatic isogenic and *PSEN1ΔE9* iMGLs, whereas sA $\beta$  had no effect (Figures 5J and 5K).

iMGLs phagocytosed also fluorescent A $\beta$ 1-42 spontaneously (Figure 5M). *APP<sup>swe</sup>* iMGLs internalized 1.2-fold more A $\beta$  compared with their controls (Figures 5N and 5O). *PSEN1ΔE9* or *APOE4* genotypes had no effect (Figure 54). To test the impact of proinflammatory activation on A $\beta$  phagocytosis, we treated the cells with LPS, sA $\beta$ , or fA $\beta$  simultaneously with fluorescent A $\beta$ . LPS reduced A $\beta$  phagocytosis only in isogenic and *PSEN1ΔE9* iMGLs (Figure 54), and fA $\beta$  induced engorged vacuoles in all genotypes (Figure 5P). In summary, iMGLs presented microglia-like phagocytosis of both particles and A $\beta$  and altered phagocytosis upon inflammatory stimuli. Only *APOE4* iMGLs showed mild impairment in phagocytosis.

### Cytokine Release under Proinflammatory Conditions Is Aggravated in *APOE4* iMGLs but Decreased in *PSEN1ΔE9* and *APP<sup>swe</sup>* iMGLs

To study cytokine release, conditioned medium was analyzed with cytokine bead array after 24 h treatment with vehicle, LPS, IFN- $\gamma$ , or LPS-IFN- $\gamma$  (Figure 6A). Under basal conditions, the levels of proinflammatory cytokines IL-6, tumor necrosis factor alpha (TNF- $\alpha$ ), regulated on activation, normal T cell expressed and secreted (RANTES), and granulocyte-macrophage colony-stimulating factor (GM-CSF) were negligible (<1 pg/mL), whereas IL-8 levels were small (10 pg/mL) and MCP1 reached even 1 ng/mL concentrations (Figure 6A). As expected, iMGLs robustly responded to LPS with significant induction in all measured cytokines. The combination of LPS-IFN- $\gamma$  triggered similar or even higher release of cytokines except GM-CSF, whereas IFN- $\gamma$  alone induced only small, yet detectable, increase.

We investigated further LPS-IFN- $\gamma$  effect since it simulates *in vivo* damage-associated molecular patterns acting on Toll-like receptors and IFN- $\gamma$  produced by CNS cells (Pulido-Salgado et al., 2018). *APP<sup>swe</sup>* iMGLs produced less TNF- $\alpha$  and MCP1 in response to LPS-IFN- $\gamma$  compared with control iMGLs (Figure 6B). Similarly, *PSEN1ΔE9* iMGLs secreted less IL-6, TNF- $\alpha$ , and RANTES compared with their isogenic controls (Figure 6C). Concomitantly, LPS or IFN- $\gamma$  alone resulted in decreased cytokine secretion in iMGLs harboring these genotypes (Figure 54). In contrast, *APOE4* iMGLs produced more cytokines compared with *APOE3* iMGLs upon treatment with LPS-IFN- $\gamma$  (Figure 6D), LPS or IFN- $\gamma$  (Figure 54). Taken together, *APOE4* genotype increased cytokine secretion, whereas FAD mutations reduced it.

### Metabolism of iMGLs Is Altered under Pro- and Anti-inflammatory Stimuli and by *APOE4* Genetic Background

To investigate metabolism under anti- or proinflammatory stimuli we measured the cellular respiration of iMGLs after 24 h treatment with IL-4, LPS, IFN- $\gamma$ , or LPS-IFN- $\gamma$  (Figures 7A and 7B). An anti-inflammatory IL-4 increased parameters of oxidative respiration, whereas proinflammatory LPS and LPS-IFN- $\gamma$  reduced them (Figure 7C). IFN- $\gamma$  increased all parameters except ATP production (Figure 7C). Compared with LPS, LPS-IFN- $\gamma$  reversed oxidative parameters toward the levels of the vehicle (Figure 7C). On the contrary, all proinflammatory stimuli increased anaerobic glycolysis and glycolytic capacity indicating a shift from oxidative respiration toward anaerobic glycolysis (Figure 7D). The pooled data for LPS normalized to the vehicle confirmed the equal shifts in all genotypes, except the proton leak was increased in pAPP and glycolytic capacity in spAPP compared with control iMGLs (Figure 7E).

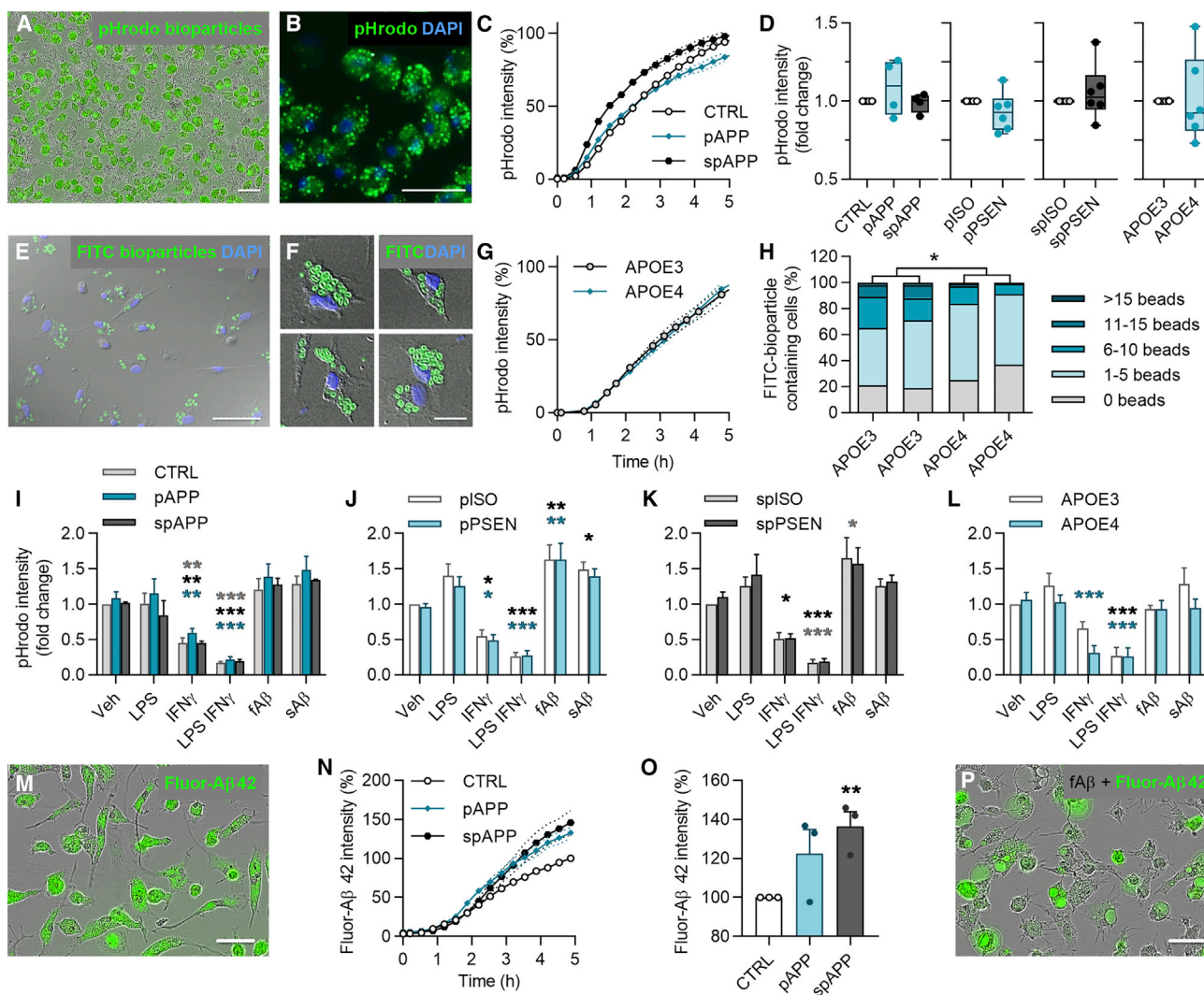


**Figure 5. Phagocytosis Is Dampened in *APOE4* iMGLs, but not in *APPswe* or *PSEN1ΔE9* iMGLs**

(A and B) Representative images of phagocytosed green pHrodo Zymosan A bioparticles in iMGLs at 5 h. (C) Time curves for pHrodo fluorescence intensity in control (CTRL) and *APPswe* (APP) iMGLs normalized to cell amount. (D) Respective boxplots at 5 h normalized to control or isogenic (ISO) iMGLs. (E and F) Representative images of phagocytosed FITC Zymosan A bioparticles in iMGLs. (G) pHrodo time curves for *APOE3* and *APOE4* iMGLs. (H) Percentages of *APOE* iMGLs that internalized certain number of FITC particles per cell.  $n = 290\text{--}750$  cells. (I–L) pHrodo intensity at 5 h, after 24 h pretreatment with 100 ng/mL LPS, 20 ng/mL IFN- $\gamma$ , or LPS-IFN- $\gamma$ , or with simultaneous treatment with 0.5  $\mu$ M soluble sA $\beta$  or fibrillar fA $\beta$ , compared with vehicle (Veh) in *APPswe* (I), pPSEN (J), spPSEN (K), and *APOE* (L) iMGLs. (M) Representative image of phagocytosed green fluor-A $\beta$ 1-42 in iMGLs at 5 h. (N) Time curves for fluorescence intensity of fluor-A $\beta$  in control and *APPswe* iMGLs. (O) Respective bar graphs at 5 h normalized to control iMGLs. (P) Representative image of iMGLs treated with fluor-A $\beta$  and fA $\beta$  depicting enlarged vacuoles. Scale bars, 50  $\mu$ m. Curve graphs show a representative experiment of 3 replicates,  $n = 4$  wells. Boxplots and bar graphs show normalized results from  $n = 2\text{--}6$  replicate batches. Data presented mean  $\pm$  SEM unpaired two-tailed t test or two-way ANOVA with Bonferroni's post hoc test, \* $p < 0.05$ , \*\* $p < 0.01$ , \*\*\* $p < 0.001$ . p, presymptomatic; sp, symptomatic; PSEN, *PSEN1ΔE9* iMGLs. See also Figure S4.

To elucidate whether AD-predisposing genetic backgrounds provoked a metabolic shift toward a proinflammatory glycolytic phenotype, we next compared respiration

between the genotypes without stimulus. FAD mutations did not alter the metabolism (Figures 7F and 7G). In contrast, oxygen consumption rate was lower in *APOE4*



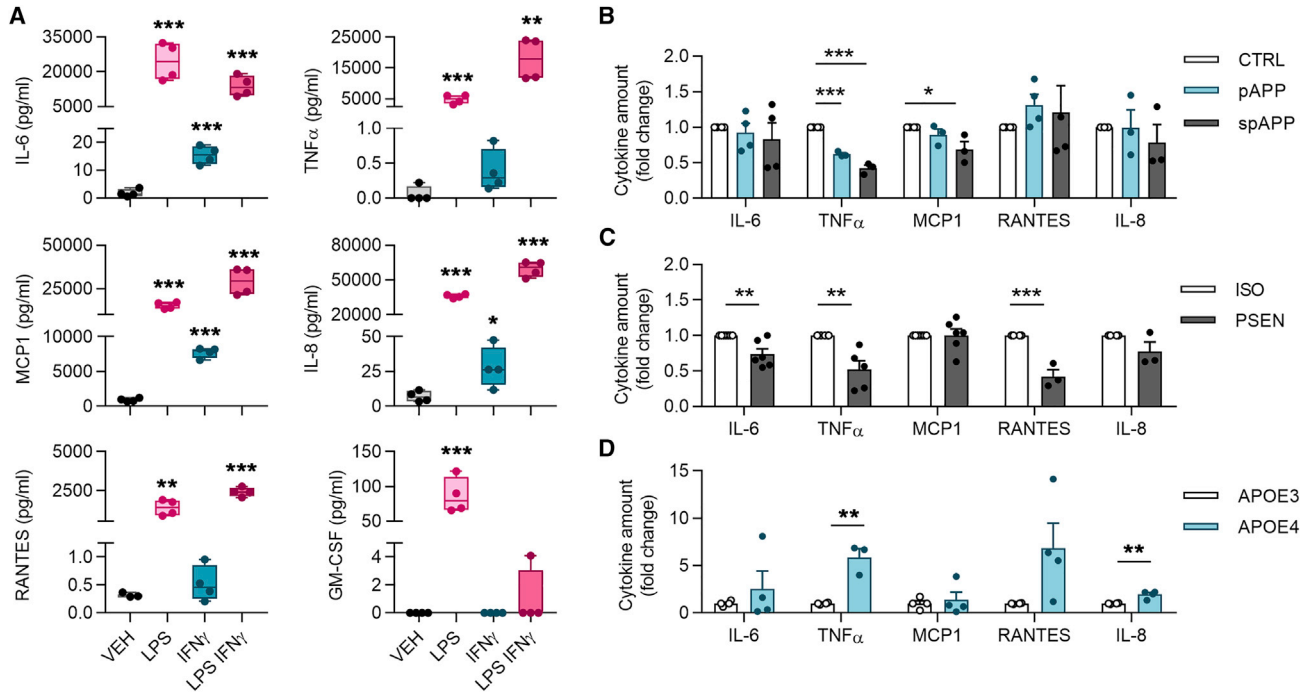


**Figure 6. Cytokine Release under Proinflammatory Conditions Is Aggravated in *APOE4* iMGLs but Decreased in *PSEN1ΔE9* and *APPswe* iMGLs**

(A) iMGLs secrete cytokines when stimulated for 24 h with LPS 100 ng/mL, IFN- $\gamma$  20 ng/mL, or their combination LPS-IFN- $\gamma$  as measured from media by cytometric bead array assay. Representative graphs. n = 4 wells.

(B) spAPP iMGLs released less TNF- $\alpha$ , and pAPP less TNF- $\alpha$  and MCP1, compared with control iMGLs in response to LPS-IFN- $\gamma$  treatment.

(C) *PSEN1ΔE9* iMGLs released less IL-6, TNF- $\alpha$ , and RANTES compared with isogenic iMGLs.

(D) In contrast, *APOE4* iMGLs released aggregated amounts of TNF- $\alpha$  and IL-8 compared with *APOE3*. For (B–D) n = 3–6 batches, each with 4 wells.

Data presented mean  $\pm$  SEM unpaired two-tailed t test, \*p < 0.05, \*\*p < 0.01, \*\*\*p < 0.001. See also Figure S4. CTRL, control; p, presymptomatic; sp, symptomatic; PSEN, *PSEN1ΔE9*; APP, *APPswe*; and ISO, isogenic control iMGLs.

iMGLs compared with *APOE3* iMGLs, demonstrating a similar shift as with LPS treatment (Figure 7H). Surprisingly, the *APOE4* genotype led to a reduced extracellular acidification (Figure 7H), whereas LPS had increased it (Figure 7A). In accordance, *APOE4* iMGLs showed a reduction in all mitochondrial parameters compared with the *APOE3* iMGLs (Figure 7I).

## DISCUSSION

Here, we demonstrate the power of iPSC-derived microglia to elucidate distinct functional phenotypes of human microglia in disease. Differentiated iMGLs show a typical microglia-like gene and protein expression and respond to inflammatory stimuli robustly in multiple functional assays. We pinpoint specific phenotypes in iMGLs with three AD-predisposing genetic backgrounds, revealing that *APOE4* has a profound impact on several aspects of microglial functionality, whereas *APPswe* and *PSEN1ΔE9* have

minor effects. The distinct phenotypes were observed without changes in amounts of A $\beta$ , suggesting that A $\beta$  burden associated with *PSEN1ΔE9*, *APPswe*, and *APOE4* is of neuronal and astrocytic origin (Oberstein et al., 2015; Scheuner et al., 1996), and that human microglia with these genotypes harbor alternative mechanisms underlying development and progression of AD.

This study reveals that *APOE4* iMGLs are fundamentally unable to mount normal microglial functionality as hypothesized for AD (Saijo and Glass, 2011). The *APOE4* genotype impaired phagocytosis and migration, and aggravated inflammatory responses of iMGLs, suggesting that *APOE4* confers iMGLs toward a proinflammatory disease-associated microglial (DAM) phenotype (Lin et al., 2018; Olah et al., 2018). We also reported similar responses to proinflammatory IFN- $\gamma$  and LPS in phagocytosis and cytokine release, consistent with murine microglia (Townsend et al., 2005; Koenigsnecht-Talboo and Landreth, 2005). *APOE4* conferred decrease in migration at basal level and in response to fractalkine, although no changes in

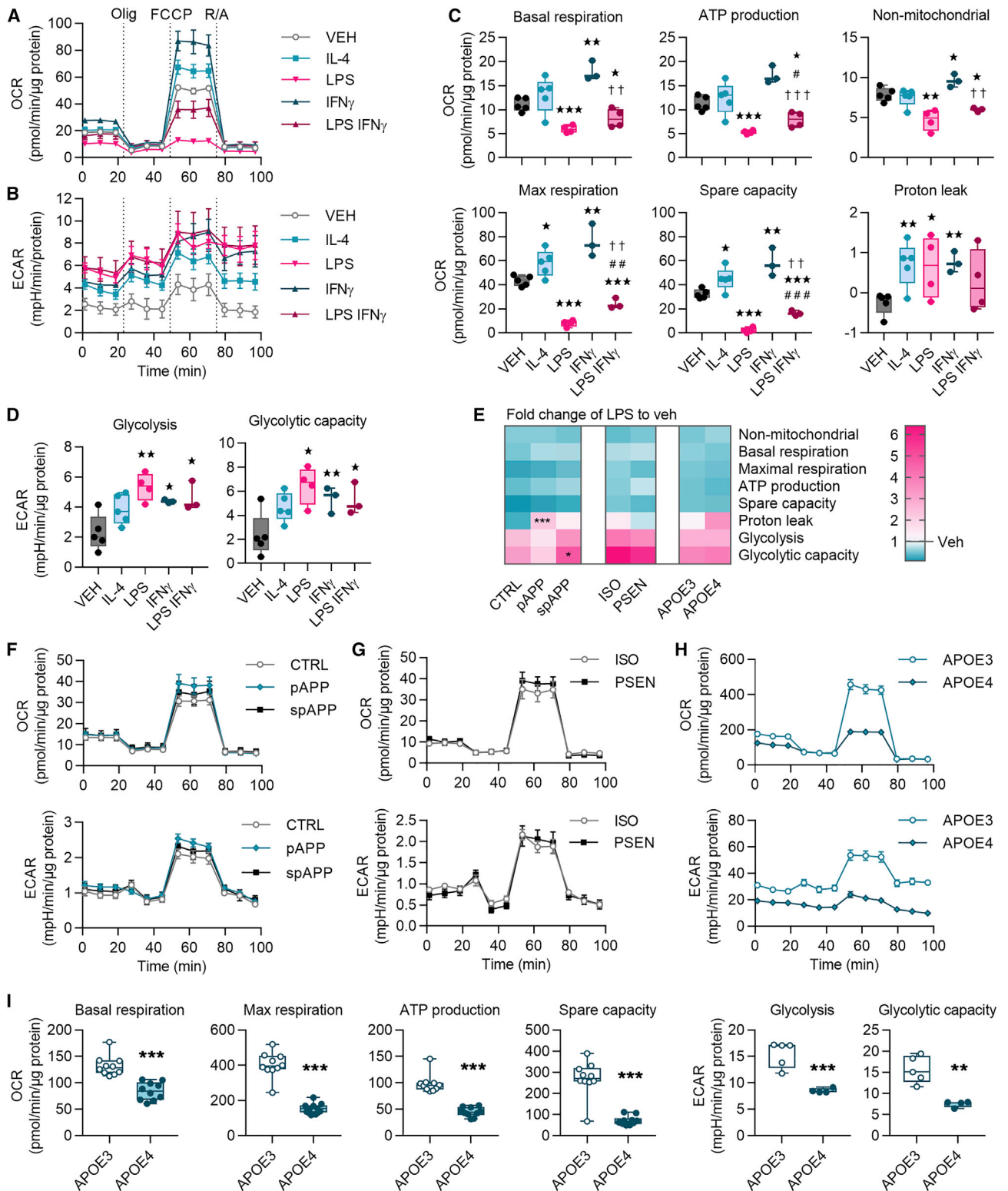


**Figure 7. Metabolism of iMGLs Is Altered under Pro- and Anti-inflammatory Stimuli and by *APOE4* Genetic Background**

(A) Representative oxygen consumption rate (OCR) curves for iMGLs following 24 h vehicle (VEH), LPS, IL-4, IFN- $\gamma$ , and LPS-IFN- $\gamma$  treatments, all 20 ng/mL. n = 3–5 wells.

(legend continued on next page)



P2RY12 or CX3CR1 expression were observed. Furthermore, no increase in chemokinesis upon A $\beta$  exposure was seen in scratch wound assay, although invasion assays could be more relevant to study chemotaxis. In mouse models, the switch to DAM is triggered by TREM2-APOE interaction (Krasemann et al., 2017); however, exact mechanisms underlying human *APOE4*-induced inflammatory phenotype in AD microglia remain incompletely defined.

We extend these findings to highlight a novel role of *APOE4* in impaired metabolism of microglia. The cellular metabolism was robustly shifted in all iMGLs in response to inflammatory stimuli. LPS induced switch from oxidative metabolism to anaerobic glycolysis in line with recent evidence (Ghosh et al., 2018; Orihuela et al., 2016), whereas less studied IFN- $\gamma$  increased both oxidative and glycolytic metabolism, supporting its role in the priming of microglia to meet the energy demands upon activation (Ta et al., 2019). Metabolic shift toward glycolysis is reported to occur also in AD microglia with *TREM2* mutations (Ulland et al., 2017). On the contrary, we observed a general downregulation of all metabolic parameters, both oxidative and glycolytic, in *APOE4* iMGLs. Thus, *APOE4*-induced inhibition of microglial metabolism and phagocytosis accompanied with heightened cytokine release may partly explain the development AD-related plaque burden in the brain.

In contrast to *APOE4*, the FAD mutations caused only a slight decrease in proinflammatory cytokine release and increase in chemokinesis. Unlike that recently reported for sporadic AD lines (Xu et al., 2019), *APP<sup>swe</sup>* and *PSEN1ΔE9* mutations did not predispose iMGLs toward a more proinflammatory phenotype, but rather toward a senescent phenotype incapable of implementing a full inflammatory response. Cytokine-mediated inflammation has been strongly established in multiple animal models of AD, but human patients show varied results (Wang et al., 2015; Smith et al., 2012; Barroeta-Espar et al., 2019). *PSEN2* rather than *PSEN1* has been reported to modulate microglial cytokine release (Jayadev et al., 2013). iMGLs secreted similar levels of cytokines with human autopsy microglia (Rustenhoven et al., 2016), and decrease in FAD iMGLs is consistent with lower cytokine levels reported

in certain brain areas of AD patients compared with non-AD subjects (Lanzrein et al., 1998). These mild and opposite outcomes in iMGLs with FAD mutations compared with the *APOE4* genotype indicate that functionality of human microglia with different genetic backgrounds is sensitively and distinctly modulated, and that pathogenic effects of *APP<sup>swe</sup>* and *PSEN1ΔE9* are mainly mediated by other cell types.

To elucidate the aforementioned functional AD phenotypes of human microglia we used a novel method to generate iMGLs. Several groups have recently reported protocols (Douvaras et al., 2017; Haenseler et al., 2017; Muffat et al., 2016; Pandya et al., 2017) to produce microglia from stem cells, and our protocol closely resembles methods from the Blurton-Jones group (Abud et al., 2017; McQuade et al., 2018). In our method, differentiation is initiated simply with a defined number of single cells to generate functional high-purity microglia-like cells in 24 days with a 20-fold yield. Importantly, we confirmed that most cells differentiate through primitive EMPs, the most critical step making microglia distinct from other tissue macrophages (Kennedy et al., 2007; Sturgeon et al., 2014). In our hands, low oxygen conditions during the early stages were pivotal in yielding considerable numbers of primitive EMPs, even though a recent study (McQuade et al., 2018) suggests that normoxic conditions would be advantageous for simplifying equipment. The microglia-like identity of iMGLs was confirmed with high expression of microglial signature genes and low expression of macrophage genes, since microglial genes are expressed to some extent also in primitive macrophages (Haenseler et al., 2017).

Considering that iPSC-models fundamentally produce rather immature cell types, the iMGLs probably represent relatively young microglia. In accordance, P2RY12, a marker for mature microglia, was expressed at a relatively low level (Bennett et al., 2016; Butovsky et al., 2014). iMGLs also exhibited a high migration capacity in response to chemotactic signals, such as ATP (De Simone et al., 2010; Lambert et al., 2010), as has been shown previously for young microglia (Caldeira et al., 2017). Thus, we recognize that the method can be further optimized by utilizing the advantages presented in other iPSC-derived microglia

(B–D) Corresponding extracellular acidification rate (ECAR) curves (B). Mitochondrial parameters calculated from (C) OCRs in (A and D) from ECARs in (B).

(E–H) Heatmap indicating decrease (blue) or increase (red) in fold change of mitochondrial parameters of LPS-treated iMGLs compared with vehicle (E). White equals 1.  $n = 5$  CTRL,  $n = 4$  pAPP,  $n = 2$  spAPP,  $n = 3$  *APOE3*, and  $n = 2$  *APOE4* batches with 10 wells;  $n = 1$  isogenic, and  $n = 3$  *PSEN1* batches with 4–5 wells. Representative OCR and ECAR curves for (F) control and *APP<sup>swe</sup>*, (G) isogenic and *PSEN1ΔE9*, and for (H) *APOE4* and *APOE3* iMGLs.  $n = 5$ –10 wells, repeated with three batches.

(I) Mitochondrial parameters calculated from OCRs and ECARs in (H) \* $p < 0.05$ , \*\* $p < 0.01$ , \*\*\* $p < 0.001$  compared with vehicle, #compared with LPS, †compared with IFN- $\gamma$ , two-tailed unpaired t test. Olig, oligomycin; FCCP, carbonyl cyanide-4-(trifluoromethoxy) phenylhydrazone; R/A, rotenone and antimycin A, each 1  $\mu$ M. CTRL, control; p, presymptomatic; sp, symptomatic; PSEN, *PSEN1ΔE9*; APP, *APP<sup>swe</sup>*; and ISO, isogenic control iMGLs.



protocols. FBS could be replaced with more defined supplements to reduce potential unwanted priming that might mask subtle genotype differences and additional maturation factors, such as transforming growth factor  $\beta$ , CD200, and CX3CL1, could be applied.

Taken together, we report here a short and relatively easy to use protocol to differentiate iMGLs from iPSCs. We characterize the effect of AD-predisposing genetic backgrounds on the functionality of cells featuring a profound impact of *APOE* on the phenotype of microglia. The current study highlights the importance of investigating the role of gene variants in human microglia and provides a useful, clinically relevant model for studying microglia in disease.

## EXPERIMENTAL PROCEDURES

See further details in the [Supplemental Experimental Procedures](#).

### Generation and Maintenance of iPSCs

iPSC lines Ctrl1, Ctrl3, and PSEN1, and their isogenic control lines were previously generated and characterized (Oksanen et al., 2017) by the approval of the committee on Research Ethics of Northern Savo Hospital district (123/2016) after written consent from the subjects. pAPP and spAPP lines were approved by the ethical review board of Karolinska Institutet/University (2017/834–31/1), and spAPP was characterized previously (Oksanen et al., 2018). HC1-3 and LOAD1-3 lines were characterized (Balez et al., 2016; Munoz et al., 2018; Ooi et al., 2013) with the approval of the University of Wollongong human research ethics committee (HE13/299). Previously uncharacterized lines pAPP, TOB0002c3, and MBE2968c1 were approved by the ethical review board of Karolinska Institutet/University (2017/834–31/1), or by the human research ethics committees of the Royal Victorian Eye and Ear Hospital (11/1031H, 13/1151H-004), University of Melbourne (1545394), University of Tasmania (H0014124), with the requirements of the National Health & Medical Research Council of Australia and conformed with the Declarations of Helsinki (McCaughy et al., 2016). Fibroblasts were isolated and cultured as described previously (Crombie et al., 2017; Qu et al., 2013) and were reprogrammed to iPSCs either with Sendai virus using CytoTune 1.0 kit (Invitrogen) (Holmqvist et al., 2016) or by nucleofection (Lonza Amaxa Nucleofector) (Okita et al., 2011). iPSCs were maintained in Essential 8 Medium (E8, Gibco) on Matrigel (Corning) and were passaged with 0.5 mM EDTA (Invitrogen) in the presence of 5  $\mu$ M Y-27632 (Selleckchem). All iPSCs were confirmed to be sterile and all cell cultures were tested for mycoplasma using a MycoAlert Kit (Lonza).

### Differentiation of iMGLs

On D0, iPSCs were dissociated to single cells with 0.5 mM EDTA or Accutase (Innovative Cell Technologies) and were replated at a density of 6,000–16,000 cells/cm<sup>2</sup> on Matrigel in E8, 0.5% penicillin/streptomycin (P/S) (50 IU/50 mg/mL), 5 ng/mL BMP4, 25 ng/mL Activin A (both from PeproTech or Miltenyi Bio-

tec), 1  $\mu$ M CHIR 99021 (Axon or Stem Cell Technologies) and 10  $\mu$ M Y-27632. The cells were maintained in low oxygen at 5% O<sub>2</sub>, 5% CO<sub>2</sub>, 37°C. On D1, the medium was replaced with a lower concentration of 1  $\mu$ M Y-27632. After 48 h on D2 the medium was changed to differentiation base medium (dif-base) containing DMEM/F-12, 0.5% P/S, 1% GlutaMAX, 0.0543% sodium bicarbonate (all from Thermo Fisher Scientific), 64 mg/L L-ascorbic acid and 14  $\mu$ g/L sodium selenite (both from Sigma). The dif-base was supplemented with 100 ng/mL FGF2, 50 ng/mL VEGF (both from PeproTech), 10  $\mu$ M SB431542 (Selleckchem or Stem Cell Technologies), and 5  $\mu$ g/mL insulin (Sigma). On D4, the media was replaced by dif-base supplemented with 5  $\mu$ g/mL insulin, 50 ng/mL FGF2, VEGF, IL-6, and thyroid peroxidase, and 10 ng/mL IL-3 and stem cell factor. From then on, the cells were maintained in a normoxic incubator. Fresh EMP medium was changed daily until D8, when floating round EMPs were collected from the top of the monolayer. After centrifugation 300  $\times$  g for 5 min, 350,000 cells/mL were transferred to ULA dishes (Corning) in microglial medium containing Iscove's modified Dulbecco's medium (Thermo Fisher Scientific), 0.5% P/S, and 10% heat inactivated FBS (Biowest) or DMEM/F12, 0.5% N<sub>2</sub>, 0.5% B27 supplemented with 5  $\mu$ g/mL insulin, 5 ng/mL MCSF, and 100 ng/mL IL-34 (both from PeproTech). On D10, the cell suspension was changed by centrifuging and 350,000 cells/mL were seeded back to ULA dishes in microglial maturation medium supplemented with 10 ng/mL MCSF and 10 ng/mL IL-34. This medium was changed similarly every second day until D16, when the cells were detached from ULA dishes with Accutase and replated on PDL-coated (Sigma) nunclon cell culture-treated plates (Thermo Fisher Scientific) in desired densities for experiments. Half of the maturation medium was changed daily until D23–24 when experiments were performed. To ensure the functionality of the cells after longer maturation, iMGLs from *APOE* lines were matured in presence of IL-34 (100 ng/mL) and MCSF (5 ng/mL) until D42, and similar results were obtained for cytokine secretion, qRT-PCR and phagocytosis.

### Statistical Analysis

Statistical analysis was performed using Graphpad Prism 7. Comparisons involving two groups were analyzed with two-tailed Student's t test. One-way ANOVA was utilized for comparisons with more than two groups followed by Tukey's post hoc test. Two-way ANOVA was utilized for comparisons of genotypes and treatment groups and followed by Bonferroni's multiple-comparison post hoc test. Corrected p values for multiple comparisons were reported. Differences were considered significant when  $p < 0.05$ .

### ACCESSION NUMBERS

The accession number for the RNA sequencing data generated in this paper is GEO: GSE135707. The datasets reanalyzed for this study are available through GEO: GSE89189 (Abud et al., 2017).

### SUPPLEMENTAL INFORMATION

Supplemental Information can be found online at <https://doi.org/10.1016/j.stemcr.2019.08.004>.



## AUTHOR CONTRIBUTIONS

H.K. and M.C.-S. designed and performed the experiments and analyzed the data. T.M., L.O., K.M.K., and H.K. conceived and designed the study. T.M. and H.K. developed the differentiation method of iMGLs with guidance from M.P.S. and N.P. T.M., H.K., L.O., and M.C.-S. supervised experiments and interpreted the results. D.H., A.P., A.W.H., J.V., C.G., G.C.S., S.L., J.K., and M.O. generated and characterized iPSCs lines. H.K. and M.C.-S. cultured the iPSCs and iMGLs with input from S.O., S.E., M.G.B., I.F., P.K., and M.F.F. R.G., S.C., and M.F.F. performed transcriptome analysis. I.F. developed the 3D brain organoids and M.O. prepared neuronal 3D-cultures. Y.I. and A.S. did calcium imaging. H.K. and S.W. conducted flow cytometer analysis with input from F.S. N.H., and A.W.H. performed western blots. H.K., T.M., L.O., and M.C.-S. interpreted the data and wrote the paper, while all authors provided feedback.

## ACKNOWLEDGMENTS

This work is part of an EU Joint Program – Neurodegenerative Disease Research (JPND) project. This study was funded by the University of Eastern Finland, the Academy of Finland under grant nos. 301234, 298071, 305516, and 315459 (FiNeFTD), the European Union's Horizon 2020 research and innovation program under grant agreement no. 643417, Finnish Instrumentarium Science Foundation, and Yrjö Jahnsson's Foundation grant no. 20187070, the National Health and Medical Research Council of Australia (NHMRC, APP1125796), an NHMRC Boosting Dementia Research Leadership Fellowship (APP1135720), Yulgilbar Alzheimer's Research Program, the DHB Foundation, the C.F. Leung Memorial Trust, the Brain Foundation, Dementia Australia, a National Health and Medical Research Council Practitioner Fellowship (AWH) and Senior Research Fellowship (AP, 1154389), an Australian Research Council Future Fellowship (AP, FT140100047), the University of Melbourne and Operational Infrastructure Support from the Victorian Government. We thank Matti Viitala for skin biopsies, Louise A. Rooney, Sophie Chevalier, and Maciej Daniszewski for the characterization of iPSC lines, Vikrant Singh for virtual karyotype help, and Helena H. Liang for culture of biopsies to fibroblasts. We also thank Finnish Functional Genomics Center (FFGC), University of Turku and Åbo Akademi and Biocenter Finland, for RNA sequencing.

Received: April 15, 2019

Revised: August 14, 2019

Accepted: August 15, 2019

Published: September 12, 2019

## REFERENCES

Abud, E.M., Ramirez, R.N., Martinez, E.S., Healy, L.M., Nguyen, C.H.H., Newman, S.A., Yeromin, A.V., Scarfone, V.M., Marsh, S.E., Fimbres, C., et al. (2017). iPSC-derived human microglia-like cells to study neurological diseases. *Neuron* *94*, 278–293.e9.

Bagyinszky, E., Youn, Y.C., An, S.S., and Kim, S. (2014). The genetics of Alzheimer's disease. *Clin. Interv. Aging* *9*, 535–551.

Balez, R., Steiner, N., Engel, M., Munoz, S.S., Lum, J.S., Wu, Y., Wang, D., Vallotton, P., Sachdev, P., O'Connor, M., et al. (2016). Neuroprotective effects of apigenin against inflammation, neuronal excitability and apoptosis in an induced pluripotent stem cell model of Alzheimer's disease. *Sci. Rep.* *6*, 31450.

Banati, R.B., Gehrmann, J., Czech, C., Monning, U., Jones, L.L., König, G., Beyreuther, K., and Kreutzberg, G.W. (1993). Early and rapid de novo synthesis of Alzheimer beta A4-amyloid precursor protein (APP) in activated microglia. *Glia* *9*, 199–210.

Barroeta-Espar, I., Weinstock, L.D., Perez-Nievas, B.G., Meltzer, A.C., Siao Tick Chong, M., Amaral, A.C., Murray, M.E., Moulder, K.L., Morris, J.C., Cairns, N.J., et al. (2019). Distinct cytokine profiles in human brains resilient to Alzheimer's pathology. *Neurobiol. Dis.* *121*, 327–337.

Bennett, M.L., Bennett, F.C., Liddel, S.A., Ajami, B., Zamanian, J.L., Fernhoff, N.B., Mulinyawe, S.B., Bohlen, C.J., Adil, A., Tucker, A., et al. (2016). New tools for studying microglia in the mouse and human CNS. *Proc. Natl. Acad. Sci. U S A* *113*, E1738–E1746.

Butovsky, O., Jedrychowski, M.P., Moore, C.S., Cialic, R., Lanser, A.J., Gabriely, G., Koeglsperger, T., Dake, B., Wu, P.M., Doykan, C.E., et al. (2014). Identification of a unique TGF-beta-dependent molecular and functional signature in microglia. *Nat. Neurosci.* *17*, 131–143.

Caldeira, C., Cunha, C., Vaz, A.R., Falcao, A.S., Barateiro, A., Seixas, E., Fernandes, A., and Brites, D. (2017). Key aging-associated alterations in primary microglia response to beta-amyloid stimulation. *Front. Aging Neurosci.* *9*, 277.

Colonna, M., and Butovsky, O. (2017). Microglia function in the central nervous system during health and neurodegeneration. *Annu. Rev. Immunol.* *35*, 441–468.

Crombie, D.E., Daniszewski, M., Liang, H.H., Kulkarni, T., Li, F., Lidgerwood, G.E., Conquest, A., Hernandez, D., Hung, S.S., Gill, K.P., et al. (2017). Development of a modular automated system for maintenance and differentiation of adherent human pluripotent stem cells. *SLAS Discov.* *22*, 1016–1025.

Crook, R., Verkkoniemi, A., Perez-Tur, J., Mehta, N., Baker, M., Houlden, H., Farrer, M., Hutton, M., Lincoln, S., Hardy, J., et al. (1998). A variant of Alzheimer's disease with spastic paraparesis and unusual plaques due to deletion of exon 9 of presenilin 1. *Nat. Med.* *4*, 452–455.

De Simone, R., Niturad, C.E., De Nuccio, C., Ajmone-Cat, M.A., Visentin, S., and Minghetti, L. (2010). TGF-beta and LPS modulate ADP-induced migration of microglial cells through P2Y1 and P2Y12 receptor expression. *J. Neurochem.* *115*, 450–459.

Douvaras, P., Sun, B., Wang, M., Kruglikov, I., Lallo, G., Zimmer, M., Terrenoire, C., Zhang, B., Gandy, S., Schadt, E., et al. (2017). Directed differentiation of human pluripotent stem cells to Microglia. *Stem Cell Reports* *8*, 1516–1524.

Engel, M., Balez, R., Munoz, S.S., Cabral-da-Silva, M.C., Stevens, C.H., Bax, M., Do-Ha, D., Sidhu, K., Sachdev, P., and Ooi, L. (2018). Viral-free generation and characterization of a human induced pluripotent stem cell line from dermal fibroblasts. *Stem Cell Res.* *32*, 135–138.

Ghosh, S., Castillo, E., Frias, E.S., and Swanson, R.A. (2018). Bioenergetic regulation of microglia. *Glia* *66*, 1200–1212.



- Ginhoux, F., Greter, M., Leboeuf, M., Nandi, S., See, P., Gokhan, S., Mehler, M.F., Conway, S.J., Ng, L.G., Stanley, E.R., et al. (2010). Fate mapping analysis reveals that adult microglia derive from primitive macrophages. *Science* 330, 841–845.
- Ginhoux, F., Lim, S., Hoeffel, G., Low, D., and Huber, T. (2013). Origin and differentiation of microglia. *Front. Cell Neurosci.* 7, 45.
- Haenseler, W., Sansom, S.N., Buchrieser, J., Newey, S.E., Moore, C.S., Nicholls, F.J., Chintawar, S., Schnell, C., Antel, J.P., Allen, N.D., et al. (2017). A highly efficient human pluripotent stem cell Microglia model displays a neuronal-co-culture-specific expression profile and inflammatory response. *Stem Cell Reports* 8, 1727–1742.
- Hoffmann, A., Kann, O., Ohlemeyer, C., Hanisch, U.K., and Kettenmann, H. (2003). Elevation of basal intracellular calcium as a central element in the activation of brain macrophages (microglia): suppression of receptor-evoked calcium signaling and control of release function. *J. Neurosci.* 23, 4410–4419.
- Holmqvist, S., Lehtonen, S., Chumarina, M., Puttonen, K.A., Azevedo, C., Lebedeva, O., Ruponen, M., Oksanen, M., Djelloul, M., Collin, A., et al. (2016). Creation of a library of induced pluripotent stem cells from Parkinsonian patients. *NPJ Parkinson's Dis.* 2, 16009.
- Jayadev, S., Case, A., Alajajian, B., Eastman, A.J., Moller, T., and Garden, G.A. (2013). Presenilin 2 influences miR146 level and activity in microglia. *J. Neurochem.* 127, 592–599.
- Kennedy, M., D'Souza, S.L., Lynch-Kattman, M., Schwantz, S., and Keller, G. (2007). Development of the hemangioblast defines the onset of hematopoiesis in human ES cell differentiation cultures. *Blood* 109, 2679–2687.
- Kierdorf, K., Erny, D., Goldmann, T., Sander, V., Schulz, C., Perdiguero, E.G., Wieghofer, P., Heinrich, A., Riemke, P., Holscher, C., et al. (2013). Microglia emerge from erythromyeloid precursors via Pu.1- and Irf8-dependent pathways. *Nat. Neurosci.* 16, 273–280.
- Koenigsnecht-Talboo, J., and Landreth, G.E. (2005). Microglial phagocytosis induced by fibrillar beta-amyloid and IgGs are differentially regulated by proinflammatory cytokines. *J. Neurosci.* 25, 8240–8249.
- Krasemann, S., Madore, C., Cialic, R., Baufeld, C., Calcagno, N., El Fatimy, R., Beckers, L., O'Loughlin, E., Xu, Y., Fanek, Z., et al. (2017). The TREM2-APOE pathway drives the transcriptional phenotype of dysfunctional microglia in neurodegenerative diseases. *Immunity* 47, 566–581.e9.
- Lambert, C., Ase, A.R., Seguela, P., and Antel, J.P. (2010). Distinct migratory and cytokine responses of human microglia and macrophages to ATP. *Brain Behav. Immun.* 24, 1241–1248.
- Lanzrein, A.S., Johnston, C.M., Perry, V.H., Jobst, K.A., King, E.M., and Smith, A.D. (1998). Longitudinal study of inflammatory factors in serum, cerebrospinal fluid, and brain tissue in Alzheimer disease: interleukin-1beta, interleukin-6, interleukin-1 receptor antagonist, tumor necrosis factor-alpha, the soluble tumor necrosis factor receptors I and II, and alpha1-antichymotrypsin. *Alzheimer Dis. Assoc. Disord.* 12, 215–227.
- Lavin, Y., Winter, D., Blecher-Gonen, R., David, E., Keren-Shaul, H., Merad, M., Jung, S., and Amit, I. (2014). Tissue-resident macrophage enhancer landscapes are shaped by the local microenvironment. *Cell* 159, 1312–1326.
- Lee, C.Y., and Landreth, G.E. (2010). The role of microglia in amyloid clearance from the AD brain. *J. Neural Transm. (Vienna)* 117, 949–960.
- Lin, Y.T., Seo, J., Gao, F., Feldman, H.M., Wen, H.L., Penney, J., Cam, H.P., Gjoneska, E., Raja, W.K., Cheng, J., et al. (2018). APOE4 causes widespread molecular and cellular alterations associated with Alzheimer's disease phenotypes in human iPSC-derived brain cell types. *Neuron* 98, 1141–1154.e7.
- Liu, C.C., Liu, C.C., Kanekiyo, T., Xu, H., and Bu, G. (2013). Apolipoprotein E and Alzheimer disease: risk, mechanisms and therapy. *Nat. Rev. Neurol.* 9, 106–118.
- Manocha, G.D., Floden, A.M., Rausch, K., Kulas, J.A., McGregor, B.A., Rojanathammanee, L., Puig, K.R., Puig, K.L., Karki, S., Nichols, M.R., et al. (2016). APP regulates microglial phenotype in a mouse model of Alzheimer's disease. *J. Neurosci.* 36, 8471–8486.
- McCaughy, T., Liang, H.H., Chen, C., Fenwick, E., Rees, G., Wong, R.C., Vickers, J.C., Summers, M.J., MacGregor, C., Craig, J.E., et al. (2016). An interactive multimedia approach to improving informed consent for induced pluripotent stem cell research. *Cell Stem Cell* 18, 307–308.
- McQuade, A., Coburn, M., Tu, C.H., Hasselmann, J., Davtyan, H., and Blurton-Jones, M. (2018). Development and validation of a simplified method to generate human microglia from pluripotent stem cells. *Mol. Neurodegener.* 13, 67.
- Muffat, J., Li, Y., Yuan, B., Mitalipova, M., Omer, A., Corcoran, S., Bakiasi, G., Tsai, L.H., Aubourg, P., Ransohoff, R.M., et al. (2016). Efficient derivation of microglia-like cells from human pluripotent stem cells. *Nat. Med.* 22, 1358–1367.
- Mullan, M., Crawford, F., Axelman, K., Houlden, H., Lilius, L., Winblad, B., and Lannfelt, L. (1992). A pathogenic mutation for probable Alzheimer's disease in the APP gene at the N-terminus of beta-amyloid. *Nat. Genet.* 1, 345–347.
- Munoz, S.S., Balez, R., Castro Cabral-da-Silva, M.E., Berg, T., Engel, M., Bax, M., Do-Ha, D., Stevens, C.H., Greenough, M., Bush, A., et al. (2018). Generation and characterization of human induced pluripotent stem cell lines from a familial Alzheimer's disease PSEN1 A246E patient and a non-demented family member bearing wild-type PSEN1. *Stem Cell Res.* 31, 227–230.
- Nadler, Y., Alexandrovich, A., Grigoriadis, N., Hartmann, T., Rao, K.S., Shohami, E., and Stein, R. (2008). Increased expression of the gamma-secretase components presenilin-1 and nicastrin in activated astrocytes and microglia following traumatic brain injury. *Glia* 56, 552–567.
- Oberstein, T.J., Spitzer, P., Klafki, H.W., Linning, P., Neff, F., Knolker, H.J., Lewczuk, P., Wiltfang, J., Kornhuber, J., and Maler, J.M. (2015). Astrocytes and microglia but not neurons preferentially generate N-terminally truncated Abeta peptides. *Neurobiol. Dis.* 73, 24–35.
- Okita, K., Matsumura, Y., Sato, Y., Okada, A., Morizane, A., Okamoto, S., Hong, H., Nakagawa, M., Tanabe, K., Tezuka, K., et al. (2011). A more efficient method to generate integration-free human iPSC cells. *Nat. Methods* 8, 409–412.



- Oksanen, M., Hyotylainen, I., Voutilainen, J., Puttonen, K.A., Hamalainen, R.H., Graff, C., Lehtonen, S., and Koistinaho, J. (2018). Generation of a human induced pluripotent stem cell line (LL008 1.4) from a familial Alzheimer's disease patient carrying a double KM670/671NL (Swedish) mutation in APP gene. *Stem Cell Res.* *31*, 181–185.
- Oksanen, M., Petersen, A.J., Naumenko, N., Puttonen, K., Lehtonen, S., Gubert Olive, M., Shakirzyanova, A., Leskela, S., Sarajarvi, T., Viitanen, M., et al. (2017). PSEN1 mutant iPSC-derived model reveals severe astrocyte pathology in Alzheimer's disease. *Stem Cell Reports* *9*, 1885–1897.
- Olah, M., Patrick, E., Villani, A.C., Xu, J., White, C.C., Ryan, K.J., Piehowski, P., Kapasi, A., Nejad, P., Cimpean, M., et al. (2018). A transcriptomic atlas of aged human microglia. *Nat. Commun.* *9*, 539.
- Ooi, L., Sidhu, K., Poljak, A., Sutherland, G., O'Connor, M.D., Sachdev, P., and Munch, G. (2013). Induced pluripotent stem cells as tools for disease modelling and drug discovery in Alzheimer's disease. *J. Neural Transm. (Vienna)* *120*, 103–111.
- Orihuela, R., McPherson, C.A., and Harry, G.J. (2016). Microglial M1/M2 polarization and metabolic states. *Br. J. Pharmacol.* *173*, 649–665.
- Pandya, H., Shen, M.J., Ichikawa, D.M., Sedlock, A.B., Choi, Y., Johnson, K.R., Kim, G., Brown, M.A., Elkhoulou, A.G., Maric, D., et al. (2017). Differentiation of human and murine induced pluripotent stem cells to microglia-like cells. *Nat. Neurosci.* *20*, 753–759.
- Pulido-Salgado, M., Vidal-Taboada, J.M., Barriga, G.G., Sola, C., and Saura, J. (2018). RNA-Seq transcriptomic profiling of primary murine microglia treated with LPS or LPS + IFN $\gamma$ . *Sci. Rep.* *8*, 16096.
- Qu, C., Puttonen, K.A., Lindeberg, H., Ruponen, M., Hovatta, O., Koistinaho, J., and Lammi, M.J. (2013). Chondrogenic differentiation of human pluripotent stem cells in chondrocyte co-culture. *Int. J. Biochem. Cell Biol.* *45*, 1802–1812.
- Rustenhoven, J., Park, T.I., Schweder, P., Scotter, J., Correia, J., Smith, A.M., Gibbons, H.M., Oldfield, R.L., Bergin, P.S., Mee, E.W., et al. (2016). Isolation of highly enriched primary human microglia for functional studies. *Sci. Rep.* *6*, 19371.
- Saijo, K., and Glass, C.K. (2011). Microglial cell origin and phenotypes in health and disease. *Nat. Rev. Immunol.* *11*, 775–787.
- Scheuner, D., Eckman, C., Jensen, M., Song, X., Citron, M., Suzuki, N., Bird, T.D., Hardy, J., Hutton, M., Kukull, W., et al. (1996). Secreted amyloid beta-protein similar to that in the senile plaques of Alzheimer's disease is increased in vivo by the presenilin 1 and 2 and APP mutations linked to familial Alzheimer's disease. *Nat. Med.* *2*, 864–870.
- Schwartz, M.P., Hou, Z., Propson, N.E., Zhang, J., Engstrom, C.J., Santos Costa, V., Jiang, P., Nguyen, B.K., Bolin, J.M., Daly, W., et al. (2015). Human pluripotent stem cell-derived neural constructs for predicting neural toxicity. *Proc. Natl. Acad. Sci. U S A* *112*, 12516–12521.
- Selkoe, D.J. (1998). The cell biology of beta-amyloid precursor protein and presenilin in Alzheimer's disease. *Trends Cell Biol.* *8*, 447–453.
- Shi, Y., and Holtzman, D.M. (2018). Interplay between innate immunity and Alzheimer disease: APOE and TREM2 in the spotlight. *Nat. Rev. Immunol.* *18*, 759–772.
- Smith, J.A., Das, A., Ray, S.K., and Banik, N.L. (2012). Role of pro-inflammatory cytokines released from microglia in neurodegenerative diseases. *Brain Res. Bull.* *87*, 10–20.
- Sturgeon, C.M., Ditadi, A., Awong, G., Kennedy, M., and Keller, G. (2014). Wnt signaling controls the specification of definitive and primitive hematopoiesis from human pluripotent stem cells. *Nat. Biotechnol.* *32*, 554–561.
- Ta, T.T., Dikmen, H.O., Schilling, S., Chausse, B., Lewen, A., Hollnagel, J.O., and Kann, O. (2019). Priming of microglia with IFN $\gamma$  slows neuronal gamma oscillations in situ. *Proc. Natl. Acad. Sci. U S A*. <https://doi.org/10.1073/pnas.1813562116>.
- Townsend, K.P., Town, T., Mori, T., Lue, L.F., Shytle, D., Sanberg, P.R., Morgan, D., Fernandez, F., Flavell, R.A., and Tan, J. (2005). CD40 signaling regulates innate and adaptive activation of microglia in response to amyloid beta-peptide. *Eur. J. Immunol.* *35*, 901–910.
- Uenishi, G., Theisen, D., Lee, J.H., Kumar, A., Raymond, M., Vodyanik, M., Swanson, S., Stewart, R., Thomson, J., and Slukvin, I. (2014). Tenascin C promotes hematoendothelial development and T lymphoid commitment from human pluripotent stem cells in chemically defined conditions. *Stem Cell Reports* *3*, 1073–1084.
- Ulland, T.K., Song, W.M., Huang, S.C., Ulrich, J.D., Sergushichev, A., Beatty, W.L., Loboda, A.A., Zhou, Y., Cairns, N.J., Kambal, A., et al. (2017). TREM2 maintains microglial metabolic fitness in Alzheimer's disease. *Cell* *170*, 649–663.e13.
- Wang, W.Y., Tan, M.S., Yu, J.T., and Tan, L. (2015). Role of pro-inflammatory cytokines released from microglia in Alzheimer's disease. *Ann. Transl. Med.* *3*, 136.
- Weuve, J., Hebert, L.E., Scherr, P.A., and Evans, D.A. (2014). Deaths in the United States among persons with Alzheimer's disease (2010–2050). *Alzheimers Dement.* *10*, e40–e46.
- Xu, M., Zhang, L., Liu, G., Jiang, N., Zhou, W., and Zhang, Y. (2019). Pathological changes in Alzheimer's disease analyzed using induced pluripotent stem cell-derived human Microglia-like cells. *J. Alzheimers Dis.* *67*, 357–368.
- Zhang, Y., Chen, K., Sloan, S.A., Bennett, M.L., Scholze, A.R., O'Keefe, S., Phatnani, H.P., Guarnieri, P., Caneda, C., Ruderisch, N., et al. (2014). An RNA-sequencing transcriptome and splicing database of glia, neurons, and vascular cells of the cerebral cortex. *J. Neurosci.* *34*, 11929–11947.
- Zhao, Y., Li, X., Huang, T., Jiang, L.L., Tan, Z., Zhang, M., Cheng, I.H., Wang, X., Bu, G., Zhang, Y.W., et al. (2017). Intracellular trafficking of TREM2 is regulated by presenilin 1. *Exp. Mol. Med.* *49*, e405.